

Random lasing from Anderson attractors

Guillaume Rollin¹, José Lages¹, and Dima L. Shepelyansky^{1,2}

¹*Institut UTINAM, UMR 6213, CNRS, Université Bourgogne Franche-Comté, 25000 Besançon, France*

²*Laboratoire de Physique Théorique, Université de Toulouse, CNRS, UPS, 31062 Toulouse, France*



(Received 11 January 2022; accepted 25 April 2022; published 10 May 2022)

We introduce and study a two-dimensional dissipative nonlinear Anderson pumping model that is characterized by localized or delocalized eigenmodes in a linear regime and in addition includes nonlinearity, dissipation, and pumping. We find that above a certain pumping threshold, the model has narrow spectral lasing lines generated by isolated clusters of Anderson attractors. With the increase of the pumping, the lasing spectrum is broadened even if narrow lasing peaks are still well present in the localized phase of linear modes. In the metallic phase, the presence of narrow spectral peaks is significantly suppressed. We argue that the model captures the main features observed for random lasers.

DOI: [10.1103/PhysRevA.105.053506](https://doi.org/10.1103/PhysRevA.105.053506)

I. INTRODUCTION

The theory of random lasing in disordered active media was introduced by Letokhov [1]. At present, various types of random lasers operating in different gain and scattering media, including powder and fibers, have been experimentally realized as discussed and reviewed in [2–6]. The active interest in random lasers is stimulated not only by their technological applications but also by a variety of interdisciplinary links to other research fields, such as the theory of disordered and mesoscopic systems [7], Anderson localization and transport [8,9], nonlinear waves in disordered media [10,11], chaotic dynamics and strange attractors [12,13], synchronization [14], material science, spectroscopy, and laser physics (see, e.g., [15]).

Due to such an interdisciplinary nature and complexity of random lasing systems, deep theoretical studies are required with applications of advanced analytical and numerical tools and methods. Various numerical studies have been reported with the main objective to explain specific features of random lasing observed in experiments (see, e.g., [16–18]). Thus in [16] diffusive multimode random lasers have been analyzed theoretically in the frame of a time-independent self-consistent approach. A statistical theory of strongly coupled Anderson-localized modes has been applied within a dyadic Green's function formalism in a one-dimensional (1D) approximation [17]. A semiclassical theory for multimode random lasing has been used in the frame of Maxwell-Bloch equations in 1D systems for the analysis of lasing from Anderson localized modes [18]. In a certain sense, these approaches are based on steady-state self-consistent solutions of nonlinear equations.

However, for random lasing it is important to study the time-dependent complex dynamics with an interplay of nonlinearity, disorder, dissipation, and pumping which may not be reducible to steady-state solutions, as happens to be the case for chaotic strange attractors in generic nonlinear dis-

sipative equations with energy pumping (see, e.g., [12,13]). The properties of such chaotic dynamics are rather difficult to capture and investigate in studies of specific modeling of an experimental setup. Due to these reasons, we introduce here a simplified two-dimensional (2D) dissipative nonlinear Anderson pumping (DINAP) model that in various limiting regimes describes such generic phenomena as Anderson localization, transport in disordered media, nonlinear waves, dissipation, pumping, synchronization, and chaotic dissipative dynamics. We show that a lasing in such a model captures the main qualitative features of random lasers. A somewhat similar model was studied in [19] for the 1D case. However, the 1D case is rather far from a typical experimental situation where random lasing takes place at least in 2D systems, as in [4,5]. Also, the spectrum of lasing and lasing clusters were not studied in [19].

II. MODEL DESCRIPTION

The DINAP model is described by the time evolution equations

$$\begin{aligned} i\dot{A}_{x,y} = & E_{x,y}A_{x,y} + \beta|A_{x,y}|^2A_{x,y} + (1 - i\eta)(-A_{x,y+1} \\ & + 4A_{x,y} - A_{x,y-1} - A_{x+1,y} - A_{x-1,y}) \\ & + i(\alpha - \sigma|A_{x,y}|^2)A_{x,y}. \end{aligned} \quad (1)$$

Here, $A_{x,y}$ is the radiation field amplitude on the site (x, y) of an $N \times N$ square lattice with periodic boundary conditions, and $E_{x,y}$ are on-site unperturbed energies randomly distributed in the $[-W/2, W/2]$ interval.

Thus, the W parameter characterizes the strength of disorder in a given system, and it determines the Anderson localization length in absence of nonlinearity, dissipation and activation. The physical processes of linear damping, or the dissipative coupling constant, are characterized by the parameter η , and the nonlinear effects of damping are characterized by the parameter σ . In addition, the lasing generation is

characterized by instability related to a pumping rate with a characteristic parameter α . With these parameters, the proposed DINAP model describes the average characteristics of random lasing, including the spontaneous emission processes as discussed in [1,3,6]. We note that this model has typical parameter features broadly used for a description of active, dissipative, and nonlinear media discussed in [6,14]. However, an additional element is the presence of disorder and Anderson localization, which are usually absent in the models discussed in [6,14].

For $\beta = \eta = \alpha = \sigma = 0$, the model is reduced to the two-dimensional Anderson model (see, e.g., [9]) with a unit hopping amplitude on nearby sites. In the absence of disorder, i.e., at $W = 0$, the spectrum of linear waves on a lattice of size $N \times N$ has the form $\lambda_{q_x, q_y} = 4 - 2 \cos(2\pi q_x/N) - 2 \cos(2\pi q_y/N)$, where q_x and q_y are wave numbers of ballistic waves [7,9]. In the presence of disorder, i.e., $W > 0$, all the eigenstates are exponentially localized on an infinite size lattice, but the localization length increases exponentially with a decrease of the disorder strength W [7,9]. For a lattice of finite size N , the localization length and the number of lattice sites effectively contributing to an eigenstate should be compared with the actual size N . For a lattice of finite size $N \sim 100$, the eigenstates are well localized at $W = 6\text{--}8$, since the number of sites contributing to eigenstates is significantly smaller than the total number of sites $N \times N$ [20]. In contrast, for $W = 3$ this number of sites becomes comparable with $N \times N$ and thus the eigenstates are practically delocalized over the whole available system size [20]. We also note that the effects of multiple scattering, which are important for random lasing (see, e.g., [1,2]), are well captured by the 2D Anderson model, which describes a unitary evolution for the linear case.

For finite β and $\eta = \alpha = \sigma = 0$, the DINAP model is reduced to the 2D discrete Anderson nonlinear Schrödinger equation (DANSE) model, which was actively studied to investigate the effects of weak nonlinearity on Anderson localization (see, e.g., [21–23]). It was shown that a moderate nonlinearity leads to a destruction of the localization and a subdiffusive spreading of the field over the lattice.

The DINAP model has several new features compared to the unitary DANSE model. Indeed, the parameter α describes lasing instability of the nonlinear media, which is balanced by the linear damping η -term and the more significant nonlinear damping σ -term. As a result, the DINAP model captures various nontrivial features of the nonlinear lasing in dissipative media with disorder. Due to nonlinearity and disorder, it is natural to expect that the dynamics will be characterized by the presence of chaotic attractors, which are typical for nonlinear dissipative systems [12,13]. We also note that the DINAP model describes the case of direct instantaneous interactions leaving aside the effects of delay and feedback.

We note that a similar model in one dimension was studied in [19]. A number of interesting results were reported there. In our studies, we analyze a more realistic 2D case, and we concentrate the investigations on the lasing spectrum produced by the nonlinear media of the DINAP model. We note the important differences of our DINAP model studies with those of [19]: we study the 2D case, which is much more adapted to the reality of random lasers, and we also concentrate our

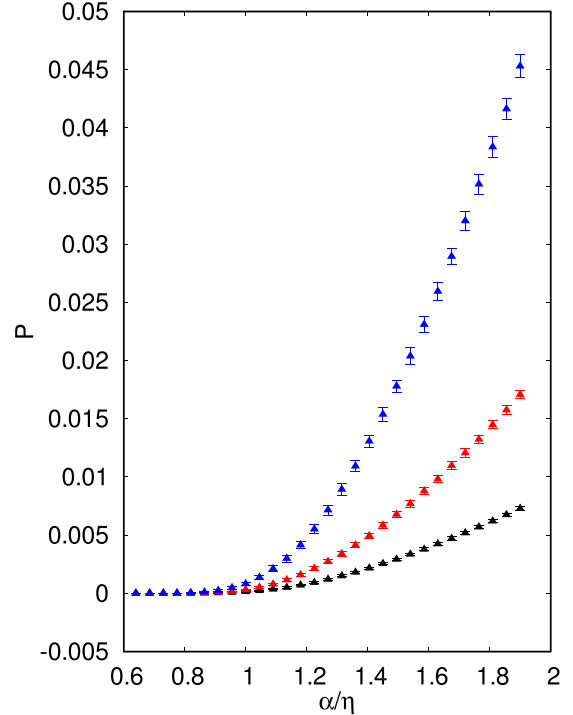


FIG. 1. Dependence of the space-averaged steady-state field power $P = \langle |A_{x,y}|^2 \rangle$ on the active media parameter α/η . Here, the parameters are $W = 8$, $\beta = \sigma = 1$. For $\eta = 0.1$, the steady state is obtained at $t_e = 10^4$ with an averaging over time interval $\Delta t = 10^3$. The lattice size is 128×128 . The values of the linear damping are $\eta = 0.2$ (blue points), $\eta = 0.1$ (red points), and $\eta = 0.05$ (black points).

analysis on the properties of the lasing spectrum, which was not analyzed in [19].

The numerical integration of the coupled equations (1) is done in the frame of the Trotter decomposition used in [21,22]. This integration scheme is symplectic (at $\eta = \alpha = \sigma = 0$) and allows us to perform accurate numerical simulations on large timescales. The physical arguments that explain the accuracy and the advantages of such integration are described in [24].

In the numerical simulations, we usually use the integration time step, $\Delta = 0.1$, checking that the variation of this step by several times is not affecting the obtained results. The main part of the results is presented for the lattice size $N \times N = 128 \times 128$. Such a size is significantly larger than the localization length of linear eigenstates with a typical disorder strength $W = 8$.

At the initial time $t = 0$, a field $A_{x,y}$ is taken as random with typical amplitudes $|A_{x,y}|^2 \approx 7 \times 10^{-11}$ with a standard deviation being approximately 4×10^{-11} . For a fixed random configuration of the energies $E_{x,y}$, the initial field amplitudes do not influence the field amplitudes at large times $t \sim 10^5$ (steady state) since the field time evolution converges to fixed Anderson attractors distributed on the lattice. This Anderson attractor steady state, averaged over a moderate time interval $\Delta t \sim 10^3$, is independent of the above described initial random field realization $A_{x,y}$.

The obtained numerical results are described in the next section.

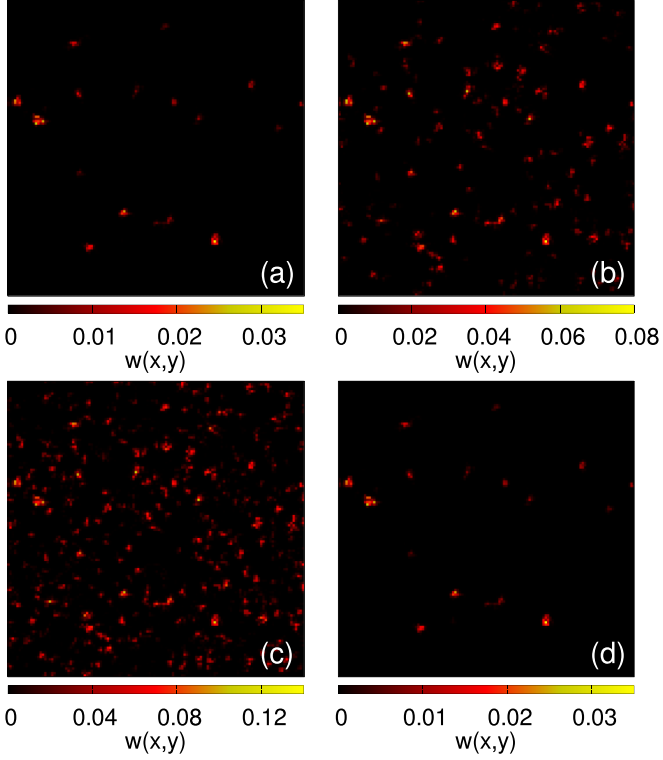


FIG. 2. Anderson attractor in the DINAP model for a 2D lattice with a linear size $N = 128$, a disorder strength $W = 8$, $\beta = \sigma = 1$, and $\eta = 0.1$. The different panels show the lasing power distribution $w(x, y) = |A_{x,y}|$ for the pumping strength $\alpha = 0.09$ (a), (d), $\alpha = 0.11$ (b), and $\alpha = 0.13$ (c). The lasing power distributions are shown after an evolution time $t_e = 10^4$ (a), (b), (c) and $t_e = 10^5$ (d). Panel (d) shows the attractor stability for long evolution times. The color bars give the values of $w(x, y)$. The $w(x, y)$ distributions are averaged over a time interval $\delta t = 10^3$.

III. RESULTS

In Fig. 1, we show the dependence of the space-averaged steady-state field power $P = \langle |A_{x,y}|^2 \rangle$ on the rescaled active media parameter α/η . The field growth is generated by an effect of active media described by the parameter α growth. The dissipative effects are produced by the η -term. The field growth is limited by the nonlinear dissipative σ -term. Thus, at small values of the ratio α/η , the generated field remains small so that $P \ll 1$ for $\alpha/\eta < 0.7$. In contrast, above the threshold value $\alpha/\eta \approx 0.7$ the field power is growing significantly, which corresponds to the random lasing regime. We note that a similar behavior has been described for the 1D model [19].

We note that the experiments with random lasing [2–4,6] are performed with rather complex media, and it is not so easy to recover from them all the parameters of the DINAP mathematical model (1). We think that the experimental dependence similar to those of Fig. 1 allows us to estimate the ratio of parameters α/η from the lasing threshold.

Typical distributions of the lasing power $w(x, y) = |A_{x,y}|^2$ on the 2D lattice are shown in Fig. 2 for different values of the activation strength α . The results show a significant increase of the number of lasing attractors with the growth of the α -parameter [see Figs. 2(a)–2(c)]. The Anderson attractor

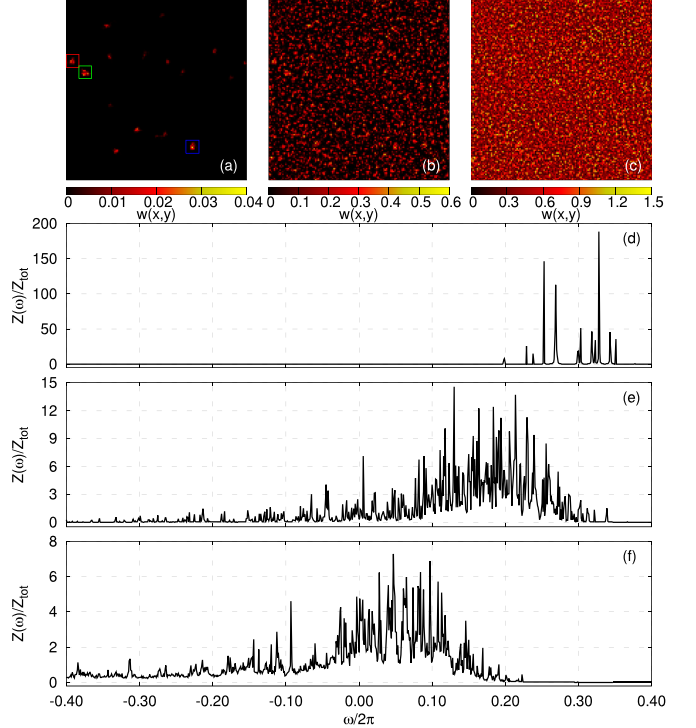


FIG. 3. Spectrum $Z(\omega)$ of random lasing in the DINAP model for a 2D lattice with a linear size $N = 128$, a disorder strength $W = 8$, $\beta = \sigma = 1$, and $\eta = 0.1$ (same parameters as in Fig. 2). The pumping strength is $\alpha = 0.09$ (a), (d), 0.31 (b), (e), and 0.91 (c), (f). Panels (a), (b), and (c) show the lasing power distributions $w(x, y)$, and panels (d), (e), and (f) show the spectrum $Z(\omega)$ of the random lasing. The integral of the spectral lasing power is $Z_{\text{tot}} \simeq 8.7 \times 10^{-8}$ (a), (d), 6.0×10^{-5} (b), (e), and 4.5×10^{-4} (c), (f). Initial conditions and random realizations are the same as in Figs. 2(a) and 2(d).

is the steady state of the system since once it is established, e.g., at $t_e = 10^4$ [see panel (a)], it continues for longer times, e.g., at $t = 10^5$ [the lasing power distributions are the same in panels (a) and (d)]. The results are shown for a typical initial field distribution with random amplitudes $A_{x,y}$ described in the previous section; we numerically check that any choice of other random configurations $A_{x,y}$ does not change the average lasing distribution.

Using the fast Fourier transform, we determine the spectrum of the random lasing defined as $Z(\omega) = \langle |\int dt A_{x,y}(t) \exp(-i\omega t)|^2 \rangle$, where the angular brackets denote the averaging over the whole lattice space. We also compute the integral of the spectral power of the random lasing $Z_{\text{tot}} = \int d\omega Z(\omega)$. The spectrum $Z(\omega)$ of the random lasing is shown in Fig. 3 together with the lasing power distribution $w(x, y)$ over the lattice. For small activation strength $\alpha = 0.09$, the lasing spectrum is composed of well-separated strong frequency peaks [Fig. 3(d)]. The space distribution [Fig. 3(a)] indicates that these frequency peaks are generated by well-separated lattice cells (clusters). We call this regime a regime of random lasing clusters. With the increase of the pumping strength $\alpha = 0.31$, the lasing spectrum becomes rather broad even if there are still a couple of dominant strong frequency peaks emerging from a quasicontinuum spectral component [Fig. 3(e)]. Over the

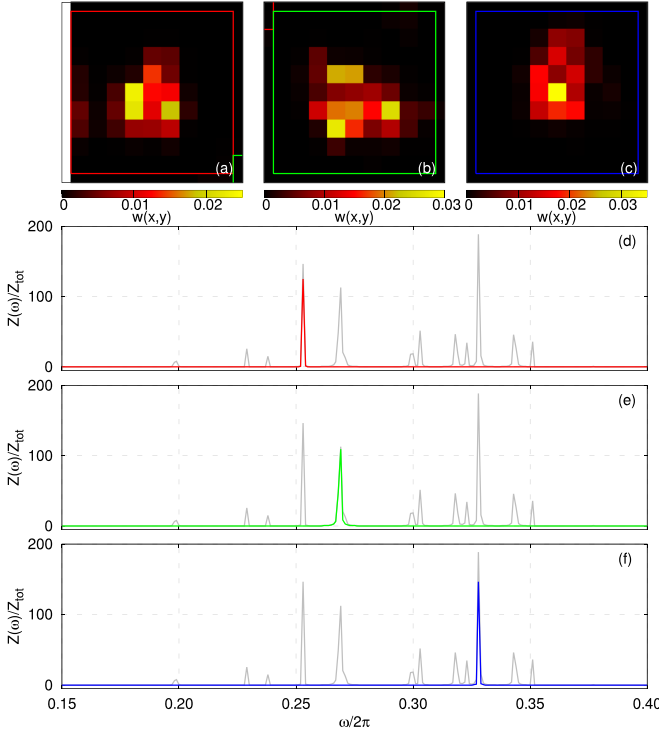


FIG. 4. The lasing clusters present in the red, green, and blue squares in Fig. 3(a) are shown in panels (a), (b), and (c), respectively. The frequencies activated by these clusters are shown by the red, green, and blue curves in panels (d), (e), and (f), respectively. The spectrum $Z(\omega)$ of the whole attractor [Fig. 3(d)] is drawn in the background of panels (d), (e), and (f). Here, the random lasing spectrum $Z(\omega)$ is normalized by the integral $Z_{\text{tot}} \simeq 8.7 \times 10^{-8}$.

lattice, see Fig. 3(b), there are more and more lasing sites as α increases. At stronger pumping strength, e.g., $\alpha = 0.91$, the lasing spectrum becomes almost continuous [Fig. 3(f)], and over the lattice, almost all the sites are lasing [Fig. 3(c)].

To demonstrate that indeed spectral peaks are generated by specific isolated clusters, we select three groups of sites for the small activation strength $\alpha = 0.09$ delimited by the red, green, and blue color squares in Fig. 3(a). In Fig. 4, we superimpose the lasing spectrum of each of the three selected clusters onto the lasing spectrum obtained for the whole lattice. The results in Fig. 4 clearly show that these three selected clusters generate well-isolated spectral peaks of lasing.

Of course, for another random realization of the on-site energies $E_{x,y}$, and for small, moderate, and strong activation strengths $\alpha = 0.09, 0.31, 0.91$, the locations of clusters are different, but the global picture of lasing is similar to those shown in Figs. 2 and 3, which describe a generic situation.

In the above presented figures, we considered the case when the linear system (i.e., the linear modes of the corresponding Anderson model) has well-localized eigenstates with a localization support being significantly smaller than the linear system size N (see the typical eigenstate characteristics for $W = 8$ in [20]). This regime is characterized by narrow peaks of the lasing spectrum generated by isolated localized clusters. It is also interesting to consider the opposite case when linear modes have a support that is comparable to the linear system size, thus corresponding to the metallic regime.

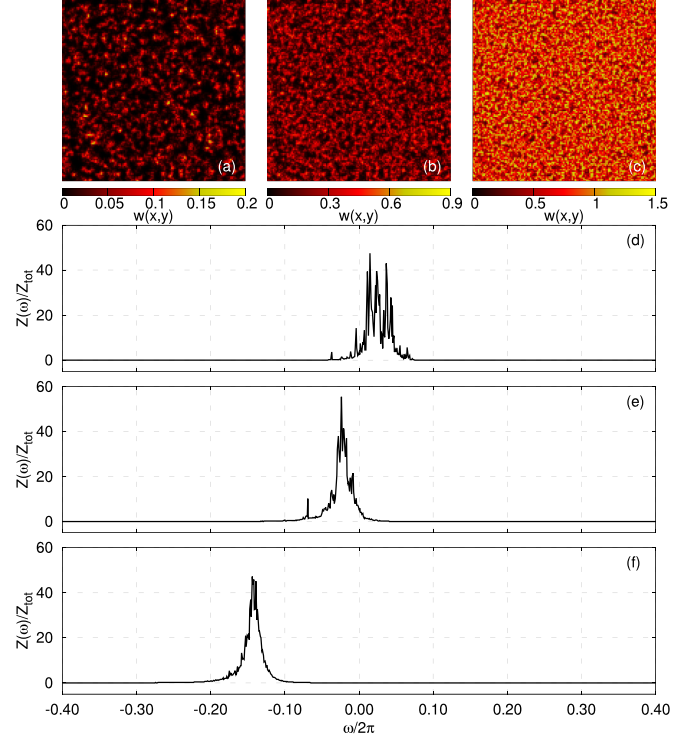


FIG. 5. Same as in Fig. 3 but for a disorder strength $W = 3$. Here, $Z_{\text{tot}} \simeq 2.41 \times 10^{-5}$ for $\alpha = 0.09$ (a),(d), 1.9×10^{-4} for $\alpha = 0.31$ (b),(e), and 7.5×10^{-4} for $\alpha = 0.91$ (c),(f).

For $W = 3$, we have approximately such a regime according to the results presented in [20]. The power distribution $w(x, y)$ over the lattice and the lasing spectrum $Z(\omega)$ for such a case are shown in Fig. 5. In this metallic regime, even for a small activation strength $\alpha = 0.09$, we have a broad spatial power distribution of lasing; the lasing spectrum is quasicontinuous. For strong activation strength $\alpha = 0.91$, almost all the lattice sites are lasing. The lasing spectrum has a structure that is similar to the one for small $\alpha = 0.09$ but with a larger number of spectral peaks. The important feature of the metallic regime at $W = 3$ is that all spectral peaks visible in the localized regime at $W = 8$ are replaced by a quasicontinuous broad distribution. Thus, the localized regime is better adapted to a narrow spectral line of lasing.

The integrated lasing power, taking the same pumping and dissipation parameters, is globally higher for the metallic phase regime [see, e.g., Figs. 5(c) and 5(f) with $W = 3$, $Z_{\text{tot}} \simeq 7.5 \times 10^{-4}$] than for the localized phase regime [see, e.g., Figs. 3(c) and 3(f) with $W = 8$, $Z_{\text{tot}} = 4.5 \times 10^{-4}$]. We attribute this to the fact that more sites contribute to the lasing in the metallic phase due to delocalized eigenstates of the linear Anderson model.

IV. DISCUSSION

We introduced a mathematical 2D DINAP model to describe specific features of the random lasers: lasing above a certain threshold, pronounced spectral lasing peaks, and lasing clusters. Our numerical analysis shows that these features are well described by the DINAP model. The important

element of the model is that in the linear regime without nonlinearity and dissipation it is reduced to the 2D Anderson model with localized modes at strong disorder and delocalized ones at weak disorder when the finite system size becomes comparable with the 2D localization length (in the infinite system). In the localized phase, above the critical pumping strength α , the spectrum of lasing is composed of narrow spectral lines. These lines emanate from localized isolated clusters located in a medium where nonlinear dissipative dynamics leads to isolated Anderson attractors. With the increase of the pumping strength, the lasing peaks are still present but a global envelope appears corresponding to lasing from a large number of connected or disconnected clusters. Globally, an increase of the pumping strength leads to a broader lasing spectrum. We find that such an effect is rather natural since with the increase of the pumping, the nonlinear frequency corrections become higher. In the metallic regime, the peaks are significantly less visible even if only slightly above the threshold pumping and at higher strength of pumping, the lasing spectrum takes the form of a smooth envelope. We attribute this feature to a delocalized structure of linear modes where nonlinear frequency corrections at high pumping get a contribution from many lattice sites on which are located the delocalized linear modes.

In the localized phase, our preliminary results show that a percolation transition takes place from a localized lasing clusters regime to a delocalized regime of lasing from many lattice sites when the strength of the pumping significantly increases above the threshold value. However, a detailed investigation of the percolation transition is beyond the scope of this work since a separate detailed study is required for this interesting phenomenon. There are a number of interesting questions about such a percolation: What is the critical percolation threshold? How does it depend on the system parameters? Is there a global synchronization of lasing, like the Kuramoto transition [14]? Is there a superradiance in such a synchronized phase? We think that the answers to these questions can be obtained with further investigations of the DINAP model.

ACKNOWLEDGMENTS

This research has been partially supported through the grant NANOX No. ANR-17-EURE-0009 (project MTDINA) in the frame of the Programme des Investissements d’Avenir, France.

-
- [1] V. S. Letokhov, Generation of light by a scattering medium with negative resonance absorption, Sov. J. Exp. Theor. Phys. **26**, 835 (1968).
 - [2] H. Cao, Lasing in random media, *Waves Random Media* **13**, R1 (2003).
 - [3] H. Cao, Review on latest developments in random lasers with coherent feedback, *J. Phys. A* **38**, 10497 (2005).
 - [4] L. Sapienza, H. Thyrrestrup, S. Stobbe, P. D. Garcia, S. Smolka and P. Lodahl, Cavity quantum electrodynamics with Anderson-localized modes, *Science* **327**, 1352 (2010).
 - [5] J. Liu, P. D. Garcia, S. Ek, N. Gregersen, T. Suhr, M. Schubert, J. Mork, S. Stobbe, and P. Lodahl, Random nanolasers in the Anderson localized regime, *Nat. Nanotechnol.* **9**, 285 (2014).
 - [6] S. K. Turitsyn, S. A. Babin, D. V. Churkin, I. D. Vatnik, M. Nikulin, and E. V. Podivilov, Random distributed feedback fibre lasers, *Phys. Rep.* **542**, 133 (2014).
 - [7] E. Akkermans and G. Montambaux, *Mesoscopic Physics of Electrons and Photons* (Cambridge University Press, Cambridge, 2007).
 - [8] P. W. Anderson, Absence of diffusion in certain random lattices, *Phys. Rev.* **109**, 1492 (1958).
 - [9] F. Evers and A. D. Mirlin, Anderson transitions, *Rev. Mod. Phys.* **80**, 1355 (2008).
 - [10] S. A. Gredeskul and Y. S. Kivshar, Propagation and scattering of nonlinear waves in disordered systems, *Phys. Rep.* **216**, 1 (1992).
 - [11] S. E. Skipetrov, A. Minguzzi, B. A. van Tiggelen, and B. Shapiro, Anderson Localization of a Bose-Einstein Condensate in a 3D Random Potential, *Phys. Rev. Lett.* **100**, 165301 (2008).
 - [12] A. J. Lichtenberg and M. Lieberman, *Regular and Chaotic Dynamics* (Springer, Berlin, 1992).
 - [13] E. Ott, *Chaos in Dynamical Systems* (Cambridge University Press, Cambridge, UK, 2002).
 - [14] A. Pikovsky, M. Rosenblum, and J. Kurths, *Synchronization: A Universal Concept in Nonlinear Sciences* (Cambridge University Press, Cambridge, UK, 2001),
 - [15] M. D. Levenson and S. S. Kano, *Introduction to Nonlinear Laser Spectroscopy* (Academic, New York, 1988).
 - [16] H. E. Türeci, L. Ge, S. Rotter, and A. D. Stone, Strong interactions in multimode random lasers, *Science* **320**, 643 (2008).
 - [17] H. Thyrrestrup, S. Smolka, L. Sapienza, and P. Lodahl, Statistical Theory of a Quantum Emitter Strongly Coupled to Anderson-Localized Modes, *Phys. Rev. Lett.* **108**, 113901 (2012).
 - [18] P. Stano and P. Jacquod, Suppression of interactions in multimode random lasers in the Anderson localized regime, *Nat. Photon.* **7**, 66 (2013).
 - [19] T. V. Laptyeva, A. A. Tikhomirov, O. I. Kanakov, and M. V. Ivanchenko, Anderson attractors in active arrays, *Sci. Rep.* **5**, 13263 (2015).
 - [20] J. Lages and D. L. Shepelyansky, Phase of bi-particle localized states for the Cooper problem in two-dimensional disordered systems, *Phys. Rev. B* **64**, 094502 (2001).
 - [21] A. S. Pikovsky, and D. L. Shepelyansky, Destruction of Anderson Localization by a Weak Nonlinearity, *Phys. Rev. Lett.* **100**, 094101 (2008).
 - [22] I. García-Mata and D. L. Shepelyansky, Delocalization induced by nonlinearity in systems with disorder, *Phys. Rev. E* **79**, 026205 (2009).
 - [23] T. V. Laptyeva, M. I. Ivanchenko, and S. Flach, Nonlinear lattice waves in heterogeneous media, *J. Phys. A* **47**, 493001 (2014).
 - [24] L. Ermann and D. L. Shepelyansky, Deconfinement of classical Yang-Mills color fields in a disorder potential, *Chaos* **31**, 093106 (2021).